Appl. Magn. Reson. 31, 573–589 (2007)

Applied Magnetic Resonance

Uniform Radio Frequency Fields in Loop-Gap Resonators for EPR Spectroscopy

R. R. Mett[1,2], J. W. Sidabras[1], and J. S. Hyde[1]

[1] Department of Biophysics, Medical College of Wisconsin, Milwaukee, Wisconsin, USA
[2] Milwaukee School of Engineering, Milwaukee, Wisconsin, USA

Received September 28, 2006; revised October 11, 2006

Abstract. At high frequencies, e.g., Q- and W-bands, it is advantageous to make the axial length of loop-gap resonators (LGRs) at least as long as a free-space wavelength. The opposite scaling of capacitance and inductance with LGR length suggests that the length of an LGR can be increased without limit, with the axial radio frequency (rf) field profiles and resonance frequency independent of length. This scaling is accurate for resonator dimensions much less than one free-space wavelength. When the resonator length approaches one-tenth of a free-space wavelength, the rf field uniformity degrades. From one-tenth to one free-space wavelength, computer simulations and experimental measurements show that the axial magnetic field energy density profile is peaked in the center of the LGR, gradually decreases from 25 to 50% at a distance one radius from the end, and rapidly thereafter. The nonuniformity is of two types. One type, in the vicinity of one radius of the end, is caused by the flaring of the field as it curves from the central loop to the end region, into the larger return loop(s). The other type, in the central part of the resonator, is caused by impedance mismatch at the ends of the LGR. The LGR may be viewed as a strongly reentrant (ridge) waveguide nearly open at both ends and supporting a standing wave. A transmission line model relates the central nonuniformity to the fringing capacitance and inductance at the ends of the resonator. This nonuniformity can be eliminated in several ways including modifying the ends of the LGR by adding a small metal bridge or a dielectric ring. These uniformity trimming elements increase the fringing capacitance and/or decrease the fringing inductance. With trimmed ends, LGRs can be made many free-space wavelengths long. The maximum resonator length is determined by the proximity in frequency of the fundamental LGR mode to the next highest frequency mode as well as the quality factor. Results of this theory are compared and confirmed with finite-element simulations. This theory connects the uniform LGR with the uniform field cavity resonators previously introduced by this laboratory.

1 Introduction

The loop-gap resonator (LGR) was introduced for use in electron paramagnetic resonance (EPR) spectroscopy in the simplest possible cross-sectional geometry (Fig. 1a) [1] and later extended to numerous other cross sections including those shown in Fig. 1b–d. The literature has been reviewed by Hyde and Froncisz [2] and by Rinard and Eaton [3]. Although the literature is extensive, there has been

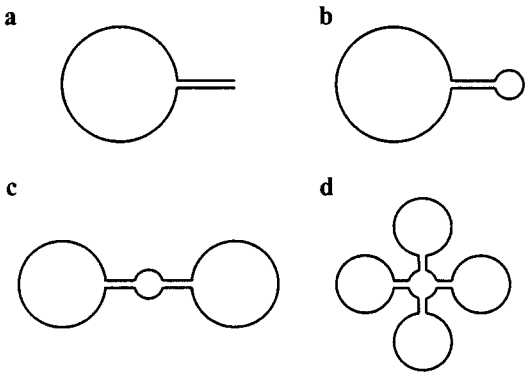

Fig. 1. LGR cross sections. **a** 1-loop–1-gap, no return flux loop. **b** 1-loop–1-gap. The sample is placed in the smaller loop and the larger loop is the flux return path. **c** 3-loop–2-gap. **d** 5-loop–4-gap.

no study of the dependence of EPR performance of LGRs on the length of the structure or on the microwave characteristics as this length approaches or exceeds the free-space (FS) wavelength. That is the subject of this paper.

LGRs in the microwave frequency range of 2 to 4 GHz were introduced as a practical alternative to cavity resonators, which are large and require too much sample in order to achieve optimum signal-to-noise ratio (SNR) [1]. The structure of Fig. 1a, a one-loop–one-gap LGR, is 4.5 mm in diameter and 10 mm in length. By adjusting the gap dimensions and introducing dielectric material into the gap, it can be made to resonate from 0.5 to 6 GHz. All dimensions are much less than a wavelength, and the structure is properly classified as a lumped circuit resonator with well-defined values of inductance L, capacitance C, and resistance R in this frequency range.

In ref. 1, data are given for two LGRs at 9.5 GHz, each with 1.2 mm diameter and 5 or 10 mm length, respectively. The rationale for use of LGRs at this frequency is that they provide superior sensitivity in comparison with cavity resonators for samples that are small. This structure is widely used in site-directed spin labeling (SDSL), where this rationale is of central importance. The quality factor Q was found to be nearly independent of length, consistent with the lumped circuit equation $Q = \omega L/R$, where ω is the resonator radian frequency, noting that both L and R are inversely proportional to resonator length. In addition, the resonant frequency was independent of cavity length, consistent with the equation $\omega = 1/\sqrt{LC}$, noting that C is proportional to length, compensating for the inverse dependence of L on length. Although the length of 10 mm is about 1/3 of a wavelength, there was no evidence that a more distributed-circuit electromagnetic-fields approach to analysis of the LGR design at 9.5 GHz was required.

The LGR design was extended to 35 GHz in a two-loop–one-gap configuration (Fig. 1b) [4] and subsequently in the three-loop–two-gap cross section of Fig. 1c [5]. In both of these designs, the sample-loop diameter (small loop) was

0.65 mm, and the length was 1 mm. In comparison with a TE_{011} resonant cavity using spin-labeled aqueous samples, SNR values were about the same, but about 10 times less sample was required with the LGR. This was found to be a useful aspect of the LGR at 35 GHz, but not nearly as critical as at 9.5 GHz because the required volume of aqueous sample for optimum performance in a cavity resonator at 35 GHz is small (about 300 nl). All dimensions of the sample loop at 35 GHz were small compared with the wavelength, and lumped-circuit models were adequate in designing the structures. An additional benefit of LGRs relative to cavity resonators was discussed in ref. 4: the phase noise voltage of microwave oscillators tends to increase linearly with microwave power [6: eq. 5.27], and at 35 GHz can be a limiting source of noise when using cavity resonators of relatively high Q values. LGRs yield good SNR even though they have low Q values because the filling factor η is very high. The low Q value reduces sensitivity to oscillator phase noise.

In a recent abstract, the LGR design of Fig. 1d for use with aqueous spin-labeled samples at 95 GHz was studied using finite-element modeling [7]. The sample-loop diameter and length were the same as used in the 35 GHz structures and resonance was achieved by reduction of the capacitance of the loops and an increase in the number of gaps (which are in series in the lumped-circuit model). At this frequency, the length of 1 mm is about 1/3 of a wavelength, the same as in the 9.5 GHz structure. At 95 GHz, sample volume in most SDSL studies will not be a problem. Theoretical comparison with a TE_{011} cavity resonator showed signal intensities to be about the same when H_1 values at the sample were the same. The rationale for use of LGRs in continuous-wave EPR at 95 GHz in order to reduce the impact of oscillator phase noise is even greater than at 35 GHz. In addition, a new benefit of the structure was identified in ref. 5: greatly increased bandwidth relative to cavity resonators. A bandwidth of 1 GHz between 3 dB points is significantly greater than the width of a rigid-limit spin-label spectrum (about 375 MHz) at this frequency, facilitating electron–electron double resonance (ELDOR) experiments.

For pulse EPR experiments, the increased bandwidth relative to cavity resonators is beneficial at all microwave frequencies because of reduced dead-time. In addition, LGRs that are relatively short in length tend to exhibit a higher efficiency parameter Λ (H_1 at the sample for 1 W incident power) relative to cavity resonators at all microwave frequencies, which is advantageous in pulse experiments.

From this overview, it is apparent that LGRs can be used over a very wide range of frequencies, although the practical benefits depend on frequency.

Until the present time, loop-gaps for use in EPR have been axially short compared to an FS wavelength. However, the opposite scaling of capacitance and inductance with LGR length suggests that the length of a LGR can be increased without limit [8]. In this lumped circuit approximation the axial radio frequency (rf) field profiles and resonance frequency are independent of length. This scaling is accurate for resonator dimensions much less than one FS wavelength. When the resonator length is increased to about a tenth of a FS wavelength, the rf

field uniformity is observed to degrade. From about one tenth to about one FS wavelength, computer simulations and experimental measurements show that the magnetic field energy density H^2 profile is axially peaked in the center of the loop-gap and decreases about 25% from the center to an axial distance equal to a radius from the end, and then drops an additional 35% at the end of the resonator. Analysis indicates that the nonuniformity is of two types. The first is in the vicinity of one radius of the end of the LGR and is caused by the flaring of the field as it goes from the central loop into the end region of the resonator, where it then extends into the larger return loops. The second type of nonuniformity is in the central part of the resonator and is caused by the LGR acting like a transmission line supporting a standing wave. The LGR may be viewed as a strongly reentrant (ridge) waveguide nearly open at both ends. A transmission line model is used to relate the central nonuniformity to the fringing capacitance and inductance at the ends of the resonator. It is found that this nonuniformity may be eliminated by adding trimming elements to the ends of the LGR. Examples include a small metal bridge or a dielectric ring placed near the gaps which increase the fringing capacitance and/or the fringing inductance. With properly designed ends, LGRs can be made many FS wavelengths long. It is found that the maximum resonator length is determined by the proximity in frequency of the lowest LGR mode to the next highest frequency mode and the quality factor. Results of this theory have been confirmed with finite-element simulations. Our results connect the LGR and the uniform field cavity resonators introduced by this laboratory [9–11]. With properly designed end sections, the loop-gap is a type of uniform field resonator.

Increased uniformity of the rf magnetic field over the sample volume produces a more uniform saturation of the sample. Benefits of this include higher EPR signal, particularly under saturable conditions. Because of smaller sample size, the benefits of using long LGRs are greater at higher rf frequencies.

2 Theory

2.1 Lumped-Circuit Model of LGR

The inductance of a circular loop of radius r and length l with current distributed uniformly in the walls and flowing perpendicular to the axis of the loop is

$$L = \mu_0 \pi r^2 / l \,, \tag{1}$$

where μ_0 is the magnetic permeability of free space. We assume that there is a central loop of radius r_i and m outer loops of radius r_o with a gap between each outer loop and the inner loop (Fig. 1b–d). The spilling of magnetic flux from both the inner and outer loops causes an increase in inductance from that predicted by Eq. (1). An accurate accounting of this effect may be made by considering problem 6.14 of Jackson [12]. In this problem, the inductance of two

parallel rectangular metal strips of width w, length l and separation t with current input on one side flowing parallel to w is given by

$$L = \mu_0 tw/(3l) .$$

This is one-third of the inductance of the shorted strips. To apply this result to the LGR, we must treat the capacitance of a gap as two capacitors in parallel divided at the location of the current null. The location of the current null is determined by conservation of flux and the size of the inductance of the inner and outer loops. To first order, we find,

$$L_i = \frac{\mu_0}{l}\left(\pi r_i^2 + \frac{mtw}{3}\frac{r_o^2}{r_o^2 + r_i^2/m}\right), \tag{2}$$

$$L_o = \frac{\mu_0}{l}\left(\pi r_o^2 + \frac{tw}{3}\frac{r_i^2/m}{r_o^2 + r_i^2/m}\right), \tag{3}$$

where the gap width and thickness (distance of separation) are given by w and t, respectively. Study of the total series impedance around the inner loop in this configuration reveals that the total inductance is a parallel combination of L_i and mL_o,

$$L_{eq} = \frac{1}{1/L_i + 1/(mL_o)} .$$

The capacitance of each gap is commonly given by

$$C = \varepsilon_0 wl/t ,$$

where ε_0 is the electric permittivity of free space. An empirical relation to account for the capacitance due to the fringing electric fields near the gap edges was introduced by the last term in eq. (3) of ref. 1. We find that the predicted resonant frequency is more accurate by about an order of magnitude (from about 10 to 1% as discussed in Sect. 3.2) when a more complicated expression for the capacitance given by Smythe [13: problem 59] is used. Smythe's model gives an exact analytic expression for the capacitance per unit length of two infinitely thin, infinitely long, parallel conducting strips of width w and distance t apart. We envision these strips as the interior metallic surfaces of the LGR gap. Neglecting end effects, which are treated in the following section, the capacitance of the two strips of length l is, in the present geometry,

$$C' = \gamma C, \tag{4}$$

where the dimensionless factor γ is given by

$$\gamma = \frac{tK(\kappa)}{wK(\sqrt{1-\kappa^2})}. \tag{5}$$

Here, K represents the complete elliptic integral of the first kind and the parameter κ in the arguments of the elliptic integral is a real number between zero and one determined by solving the equation

$$\frac{w}{t} = \frac{K(\kappa)E\{\arccos[E(\kappa)/K(\kappa)],\kappa\} - E(\kappa)F\{\arccos[E(\kappa)/K(\kappa)],\kappa\}}{E(\kappa)K(\sqrt{1-\kappa^2}) - (\sqrt{1-\kappa^2}/\kappa)^2 E(\sqrt{1-\kappa^2})K(\kappa)}. \tag{6}$$

In this equation, E of single argument represents the complete elliptic integral of the second kind while E of double argument represents the elliptic integral of the second kind. Also F represents the elliptic integral of the first kind. Equation (6) was solved numerically and Eq. (5) evaluated by Mathematica 5.0 (Wolfram Research, Inc., Champaign, IL). This model slightly underestimates the fringing capacitance because the gaps are treated as plates of zero thickness instead of the true geometry of the LGR edge.

The resonant frequency f_c of the LGR may be found from these values of inductance and capacitance,

$$f_c = 1/(2\pi\sqrt{L_{eq}C_{eq}}), \tag{7}$$

where $C_{eq} = C'/m$. A reasonable prediction of the quality factor of the empty LGR may also be found by considering the path of current flow around the loops and through the gaps with arguments similar to that used to derive the inductance,

$$Q = \omega L_{eq}/R_{eq}, \tag{8}$$

where

$$R_{eq} = \frac{1}{1/R_i + 1/(mR_o)},$$

$$R_i = \frac{2}{\sigma\delta l}\left(\pi r_i + \frac{mw}{3}\frac{r_o^2}{r_o^2 + r_i^2/m}\right),$$

$$R_o = \frac{2}{\sigma\delta l}\left(\pi r_o + \frac{w}{3}\frac{r_i^2/m}{r_o^2 + r_i^2/m}\right),$$

and where σ represents the conductivity of the metal and δ represents the skin depth in the metal of the resonator,

$$\delta = 1/\sqrt{\pi f \mu_0 \sigma}.$$

2.2 Transmission Line Model of LGR

When the length of the LGR approaches one FS wavelength, we can view the LGR as a strongly reentrant ridge waveguide with open ends. The mode of oscillation is transverse electric (TE) with the electric fields across the gaps. A TE mode in a waveguide of arbitrary cross section has a characteristic impedance [12: sect. 8]

$$Z_0 = Z_{FS}\frac{\lambda}{\lambda_{FS}}, \tag{9}$$

where $Z_{FS} = \sqrt{\varepsilon_0/\mu_0}$ is the characteristic impedance of free space, λ is the wavelength of the waveguide mode and $\lambda_{FS} = c/f$ is the FS wavelength. The guide wavelength may be expressed in terms of the cutoff frequency f_c of the mode,

$$\lambda = \lambda_{FS}/\sqrt{1-(f_c/f)^2}\,. \tag{10}$$

The cutoff frequency may be determined approximately by the lumped-circuit model (Eq. (7)) or by finite-element computer simulation.[1]

Consider a length l of waveguide with a load impedance Z_L on each end. As discussed further below, this load impedance is a high reactance from the combination of fringing electric and magnetic fields at the ends of the LGR. In order for this length of guide to resonate, the load impedance Z_L must be equal to the complex conjugate of Z_L transformed by the length l of waveguide. In terms of the guide wavenumber $k = 2\pi/\lambda$, this resonance condition may be expressed as [14]

$$\frac{Z_L^*}{Z_0} = \frac{Z_L\cos kl + iZ_0\sin kl}{Z_0\cos kl + iZ_L\sin kl}.$$

Assuming the load impedance is purely reactive, this equation may be reduced to

$$2\cot kl = \frac{\mathrm{Im}[Z_L]}{Z_0} - \frac{Z_0}{\mathrm{Im}[Z_L]}. \tag{11}$$

This equation may be solved to determine the wavenumber of each mode and the frequency through Eq. (10). Equation (11) predicts an infinite number of modes.

---

[1] A convenient approach is to use Ansoft HFSS (Ansoft Corp. Pittsburgh, PA) to obtain an eigenmode solution of a short axial slice of the LGR (waveguide) with perfect magnetic boundaries on each end.

In the limit of ideal open ends $Z_L \to \infty$ (no fringing electric or magnetic fields; or low frequencies) the solutions of Eq. (11) are

$$kl = n\pi\,, \tag{12}$$

where $n = 0, 1, 2, \ldots$. The lowest frequency mode has the solution $k = 0$ for $n = 0$ and the corresponding mode frequency is the cutoff frequency $f = f_c$. The next highest frequency mode $n = 1$ has one-half waveguide wavelength in l ($\lambda = 2l$) and each next higher frequency mode has an additional half wavelength in l. The uniformity of the rf fields along the LGR axis z is related to the wave number according to

$$(B_z, E_{\text{gap}}) \propto \begin{cases} \cos kz, & n \text{ even}, \\ \sin kz, & n \text{ odd}, \end{cases} \tag{13}$$

where $z = 0$ corresponds to the center of the resonator and $z = \pm l/2$ are the ends. The mode is uniform when $k = 0$.

In actuality, the load impedance at the end of the resonator Z_L may be modeled as a capacitance, caused by the fringing electric fields, in parallel with an inductance, caused by the fringing magnetic fields, in the end region of the LGR. For m gaps,

$$\text{Im}[Z_L] = \frac{1/m}{1/(\omega L_e) - \omega C_e}. \tag{14}$$

A convenient expression for the fringing capacitance at each end of the LGR is half the capacitance of two rectangular metal strips of dimensions w by $b - a$ a distance $2a$ apart lying in a plane and parallel along the w dimension [13: problem 58],

$$C_e = \xi \varepsilon_0 w/2\,, \tag{15}$$

where the dimensionless factor ξ is given by the ratio of complete elliptic integrals,

$$\xi = \frac{K(\sqrt{b^2 - a^2}/b)}{K(a/b)}.$$

We find that setting $a = t/2$ and $b = r_i$ produces reasonable results. The inductance of a single gap may be approximated by

$$L_e \cong \frac{\mu_0 \pi (r_i^2/m + r_o^2)}{w + r_i/m + r_o}. \tag{16}$$

For all conventional LGR designs considered, the capacitive admittance in the denominator of Eq. (14), ωC_e, is smaller than the inductive admittance $1/\omega L_e$. Then the total load reactance is large and positive. Under these conditions, the wavenumber of the $n = 0$ mode is positive, which makes the field profile slightly cosine and the mode frequency above the cutoff frequency. This behavior is observed in finite-element simulations of a wide variety of practical LGR designs at X-, Q-, and W-bands. At these frequencies the load impedance of the ends causes a nonuniformity of the mode and pulls the resonant frequency above the cutoff frequency of the LGR. In addition, the axial LGR wavelength is decreased to satisfy the resonance condition of Eq. (11). In order to make the mode uniform, capacitance may be added to the ends or inductance increased at the ends in order to produce infinite loading impedance (Eq. (14)). The condition $Z_L \to \infty$ makes the lowest frequency mode of the LGR the same as the cutoff frequency. This condition has been described extensively in publications from this laboratory about the uniform field [9–11].

We have discovered several practical ways to trim the ends of the LGR to produce uniform field for conventional LGR designs: (i) a quarter wavelength dielectric may be placed between the gaps; (ii) the gaps at the ends of the LGR may be made narrower, increasing the capacitance; (iii) a dielectric ring may be placed near the gaps to increase the capacitance; and (iv) a metal bridge may be placed near each of the gaps at the ends. Like the dielectric ring, the metal bridge also increases the fringing capacitance at the end of the LGR, but may also increase the fringing inductance by increasing the magnetic flux at the end of the LGR. Use of metal bridge elements for trimming the rf magnetic field uniformity are discussed further in Sect. 3.1.

The mode uniformity is also influenced by coupling of modes to each other by proximity in frequency and resonator Q. By using the condition

$$\frac{\Delta f}{f} \geq \frac{1}{Q},$$

where Δf is the frequency separation between modes, and estimating the frequencies of the $n = 0$ and $n = 1$ modes by Eqs. (12) and (10), an upper limit on the resonator length can be found,

$$l_{\max} \cong \frac{\lambda_{FS}}{2}\sqrt{\frac{Q}{2}}. \tag{17}$$

This has been proven accurate by finite-element modeling. If the coupler used to excite the LGR is axially symmetric, so that the $n = 2$ mode is excited and not the $n = 1$ mode, then the maximum length is double that of Eq. (17). Special designs using multiple in-phase couplers may be used to couple only to the $n = 0$ mode and further increase the maximum length of the resonator.

3 Finite-Element Simulations and Discussion

The finite-element computer program Ansoft High Frequency Structure Simulator (HFSS) (Version 10, Ansoft Corporation, Pittsburgh, PA) was used to make the numerical simulations of the modes. A HP WX8000 workstation with dual Xeon 3.2 GHz processors and 4 GB of RAM was used. The operating system was Windows 2003. The eigenmode solution method was used for all finite-element simulation results presented in this paper.

3.1 Comparison of EPR Properties of Short, Long, and Trimmed Long LGRs at Q-band

The EPR benefits of longer LGRs are illustrated by comparing properties of two Q-band 3-loop–2-gap LGRs that have been built and tested in this laboratory [15–17]. The dimensions of each LGR are shown in Table 1. The short (1 mm) LGR was made of aluminum, while the long (10 mm) was made of silver. The gap thickness of the short LGR is slightly smaller than that of the long. The resonators have no slots for modulation penetration. A mechanical drawing of the long LGR is provided in Fig. 2. No coupling structure was included in the simulations.

A comparison of the two resonators in terms of the EPR properties calculated from the finite-element simulations is shown in Table 2. The short resonator is about one-tenth of an FS wavelength and the long resonator about one. The filling factor is about 9% for the long LGR and slightly less for the short due to end effects. The filling factor is comparable to the ratio of sample volume to inner loop volume. The sample diameter could not be made larger than the indicated size without degrading the unloaded Q (Q_0) below 200. The rf magnetic field energy integrated along the LGR axis is representative of the lengths of the two resonators, which differ by a factor of 10. Cross-sectional profiles of the magnetic field energy for the two resonators are shown in Fig.

Table 1. LGR and sample dimensions.

Dimension	Value (mm) for LGR	
	Short	Long
Sample diameter d_s	0.254	0.254
Sample tube outer diameter d_t	0.330	0.330
Inner loop diameter d_i	0.648	0.660
Outer loop diameter d_o	2.06	2.06
Length l	1.016	10.03
Gap width w	1.162	1.156
Gap thickness t	0.127	0.165

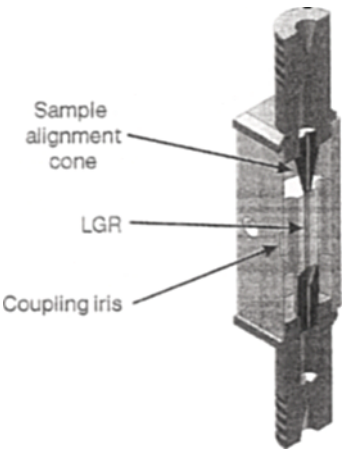

Fig. 2. Mechanical drawing of bisected 10 mm long Q-band 3-loop–2-gap LGR. The resonator body is shown in gray and the sample holder in black. Gaps face bisecting plane. The coupling iris slot appears on the nearest edge.

3a and b. The (transverse) electric fields are shown in Fig. 4. The resonator efficiency parameter is better for the short LGR by about a factor of $\sqrt{10}$. Non-saturable and saturable EPR signals were calculated from rf field integrals derived from the finite-element simulations using the methods outlined by Mett and

Table 2. Comparison of EPR properties of LGRs with sample.

Quantity	Value for LGR		
	Short	Long untrimmed	Long trimmed
d/l	0.64	0.066	0.066
l/l_{short}		9.8	9.8
l/λ_{fs}	0.118	1.15	1.14
V_{sample} (nl)	84.3	542	542
$V_{sample}/V_{inner\ loop}$ (%)	15.4	14.8	14.8
η (%)	7.59	9.42	9.15
$\int (H_z^2)_{norm}\,dz$ (mm)	1.148	9.25	10.29
$f_{no\ sample}$ (GHz)	34.965	34.481	34.158
$f_{with\ sample}$ (GHz)	34.894	34.434	34.088
$Q_{0\ no\ sample}$	650	875	863
$Q_{0\ with\ sample}$	247	234	245
Λ (G/W$^{1/2}$)	7.08	2.72	2.60
$S_{const\ P,\ nonsat}$	18.7	22.1	22.4
$(S/S_{short})_{const\ P,\ nonsat}$		1.182	1.194
$S_{const\ H,\ sat}$ (W$^{1/2}$/G)	0.936	2.88	3.04
$(S/S_{short})_{const\ H,\ sat}$		3.07	3.25

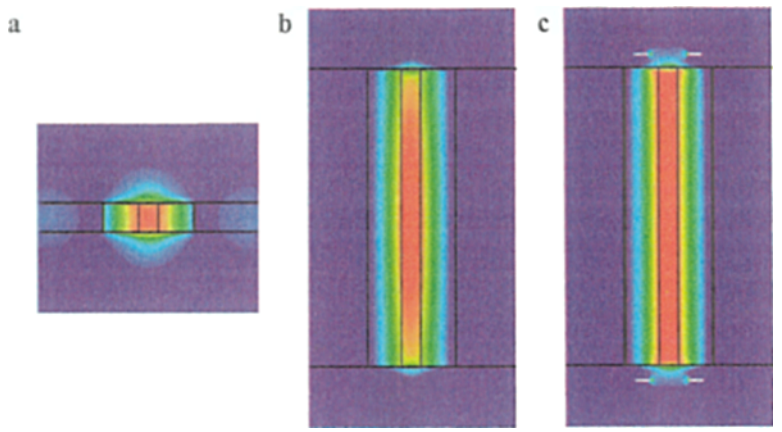

Fig. 3. Cross-sectional profiles of axial rf magnetic field energy H_z^2 in a plane bisecting the 3-loop–2-gap resonator through the gaps obtained for the $n = 0$ mode by computer simulation. Red to blue indicates maximum to zero intensity. **a** 1 mm long LGR. **b** 10 mm long LGR, untrimmed for rf magnetic field uniformity. **c** 10 mm long LGR, trimmed for rf magnetic field uniformity using metal strips bridging the gaps.

Hyde [18]. The unsaturable EPR signal (which is equal to ηQ_0) for the long LGR is better than the short by only 18% because the improvement in filling factor is nearly cancelled by a decrease in Q_0. The saturable signal, however, is improved in the longer LGR by about a factor of $\sqrt{10}$ as expected.

Also shown in Table 2 are the properties of the long LGR trimmed for axial rf magnetic field uniformity. The trimming was done by following a procedure similar to that outlined in ref. 10. First, the cutoff frequency of the long LGR with sample was found. This was done in Ansoft HFSS by taking a short axial slice of the long LGR with sample and placing a magnetic boundary on both ends. The eigenmode frequency of this structure is the cutoff frequency. Then

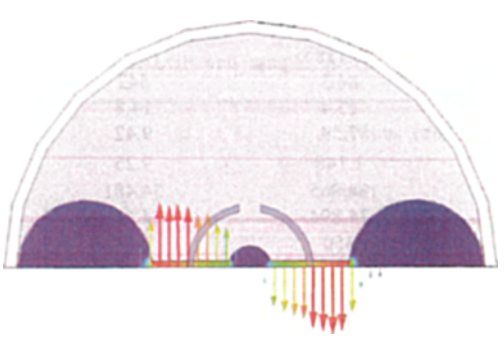

Fig. 4. Cross-sectional profile of rf electric field vectors and energy in a plane perpendicular to the axis of the 10 mm long 3-loop–2-gap resonator obtained for the $n = 0$ mode by computer simulation. Red to blue indicates maximum to zero intensity.

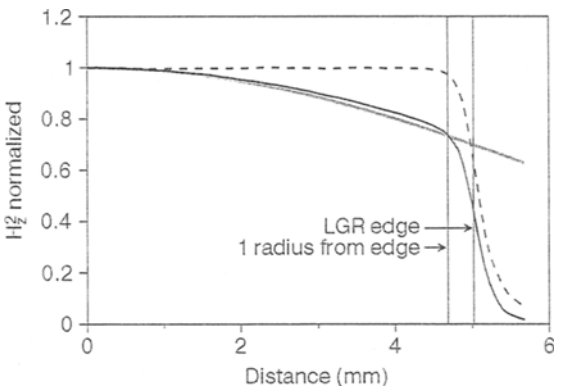

Fig. 5. Axial profiles of normalized axial magnetic field energy H_z^2 for the 10 mm 3-loop–2-gap LGR obtained by computer simulation. The three profiles correspond to the LGR untrimmed for axial magnetic field uniformity (black solid curve), trimmed for uniform axial magnetic field energy using the metal bridge (black dashed curve), and the untrimmed profile predicted by the analytic model (gray curve).

dimensions of a metal bridge were chosen (0.5 mm wide and 0.1 mm thickness [Fig. 3c]) and one bridge was centered over each gap. Each bridge has the form of a partial ring with the ends of each bridge spaced 0.33 mm apart (Fig. 3c).[2] The spacing between the bridge and gap was then adjusted until the resonant frequency of the bridged LGR was equal to the cutoff frequency. The magnetic field was then observed to be uniform. The improvement in uniformity is clearly indicated between Fig. 3b and c and in Fig. 5. The fact that this procedure produces a uniform field confirms the theory of Sect. 2.2 and connects this theory to the theory of uniform field cavity resonators introduced by this laboratory [9–11]. The distance between bridge and LGR end in this case is 0.45 mm (Fig. 3c). The metal bridge primarily increases the fringing capacitance C_e in Eq. (14) to produce $\mathrm{Im}(Z_L) \to \infty$. This lowers the resonant frequency of the LGR to the cutoff frequency through Eqs. (11) and (10). Notice the drop in frequency of the LGR from 34.434 to 34.088 GHz (Table 2). In order to accommodate this frequency shift, the LGR in most cases must be engineered for uniform field from the start, and not simply retrofitted. As seen in Table 2, the improved field uniformity produces an rf magnetic field energy integrated along the LGR nearly equal to the resonator length. The nonsaturable EPR signal is only slightly improved (by 1%), while the saturable EPR signal is improved by 6%. More significantly, the quality of the EPR signal is expected to be improved for the trimmed LGR due to uniform spin saturation.

Further confirmation of the uniform field theory of refs. 9–11 and the theory of Sect. 2.2 was observed by decreasing the spacing between the metal bridges

[2] The shape of the metal bridge is largely arbitrary; changes in shape are accommodated by changes in spacing.

and the gap. Then the rf magnetic field strength became peaked at the ends of the LGR and dipped in the center, consistent with an evanescent mode shown in fig. 5 of ref. 9 (dashed curve). In this case, the wavenumber k is imaginary since $f < f_c$ (Eq. (10)). Note that Eq. (11) remains a valid equation for the mode frequency with imaginary k because Z_0 also becomes imaginary through Eq. (9).

Field uniformity was also achieved in this LGR with the simulation process described above using other types of trimming elements, such as dielectric rings and narrowed gaps near the ends of the LGR. Uniformity was also achieved using quarter-wavelength dielectric end sections on each end of the LGR as shown in Fig. 6. In these simulations, each end of the LGR is shorted and a dielectric of axial dimension

$$d = \frac{c}{4f\sqrt{\varepsilon_r - 1}} \tag{18}$$

is placed against each shorted end. Here f is the cutoff frequency of the LGR with no dielectric (and the resonant frequency of the LGR) and ε_r is the relative dielectric constant of the dielectric. Under these conditions, the central region with no dielectric has exactly uniform field and may be made an arbitrary length as illustrated in Fig. 6. This type of resonator is a ridged analog of the uniform field cavity resonators introduced in ref. 9. Equation (18) may be de-

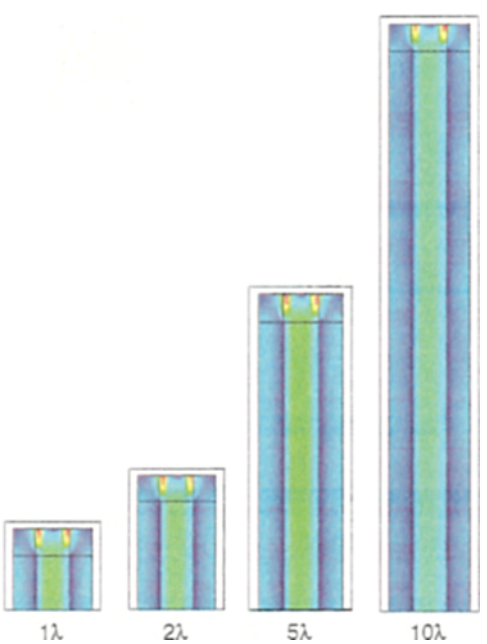

Fig. 6. Cross-sectional profiles of axial magnetic field for LGRs designed for uniform field using quarter wavelength dielectric end sections. Axial LGR lengths of different FS wavelength multiples are shown.

rived by combining Eq. (7), which yields the relationship between the cutoff frequency of the LGR with no dielectric to the cutoff frequency of the dielectric filled end sections, with Eq. (10) and setting $d = \lambda_{end}/4$. Equation (18) is identical to eq. (15) of ref. 9, which gives the size of the dielectric end sections required to produce a uniform field cavity mode. This method of producing uniform field is not practical unless modified to accommodate sample access, in which case the exact dielectric dimensions must be found by finite-element simulation.

3.2 Further Comparison of Analytic Theory and Finite-Element Simulations

The first row of Table 3 is a comparison of the cutoff frequency of the short and long LGRs obtained by finite-element simulations to those predicted by Eq. (7) with the lumped-circuit values of capacitance and inductance described in Sect. 2.1. At less than 0.8% error, agreement is better than other lumped-circuit models. Error is primarily due to the underestimate of the axial fringing capacitance at the edge of the gaps (Eq. (4)). The significantly lower cutoff frequency (2.3 GHz) of the short LGR compared to the long is caused primarily by the thinner gaps of the short relative to the long. The $n = 0$ mode frequencies of the two LGRs are similar (Table 3) as required by the EPR bridge operating frequency range. The short LGR $n = 0$ mode frequency is more strongly influenced by the fringing impedance of the ends, Eq. (14), than the long LGR. Agreement between the $n = 0$ mode frequencies predicted by HFSS and the analytic transmission line model, Eqs. (11), (10), and (14)–(16), is good for both LGRs (Table 3).

Also shown in Table 3 is a comparison of the unloaded Q values (with no sample) for the cutoff mode predicted by Eq. (8) and finite-element simulations. At about 5% error, agreement is reasonable. A comparison of higher order $n = 1$, 2, 3 mode frequencies is also shown in Table 3. Agreement is good except for the highest modes shown ($n = 1$ for the short and $n = 3$ for the long) because at over 50 GHz, the mode fields significantly spill into the end sections and

Table 3. Comparison of analytic and HFSS models for LGRs (without sample).

Quantity	Value for LGR			
	Short		Long (untrimmed)	
	HFSS	Analytic	HFSS	Analytic
f_c (GHz)	31.85	31.62	34.14	33.87
Q_c	582	620	860	895
f_0 (GHz)	34.97	35.30	34.48	34.85
f_1 (GHz)	58.81	55.21	37.68	37.36
f_2 (GHz)	–	–	44.99	41.93
f_3 (GHz)	–	–	54.68	49.57

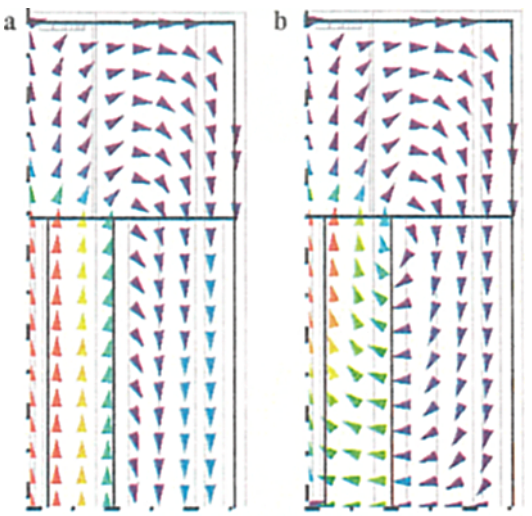

Fig. 7. Cross-sectional profiles of magnetic field vectors in a plane bisecting the 10 mm long 3-loop–2-gap resonator through the gaps obtained by computer simulation. One-quarter structure is shown. The complete structure is obtained by reflection on left and bottom edges. Red to blue indicates maximum to zero intensity. **a** $n = 0$ mode; **b** $n = 1$ mode.

therefore the lumped-circuit model of the end fringing reactance becomes inaccurate. Table 3 also shows that the frequency spacing of modes is much larger for the short LGR than for the long, consistent with Eq. (12). Comparison of the vector magnetic fields for the $n = 0$ and $n = 1$ modes for the long LGR in Fig. 7 illustrates higher-order mode behavior and is consistent with Eq. (13). The mode frequencies predicted by the transmission line model are sensitive to values of the lumped inductances and capacitances given by Eqs. (2)–(4), which influence the cutoff frequency, and Eqs. (15) and (16), which affect the placement of the modes. Figure 5 shows a comparison of the finite element and analytically predicted axial magnetic field energy density profiles after minor adjustment in end fringing capacitance.

4 Conclusions

The axial rf magnetic energy uniformity of the short and long resonators, 1 and 10 mm, respectively, differs as does the proximity of the $n = 0$ mode frequencies to the cutoff frequency and the $n = 1$ mode frequency. Nonuniformity caused by fringing capacitance has a larger effect on the shorter resonator than on the longer resonator due to the percentage of fringing capacitance over the length. Deviations of resonant frequency f from the cutoff frequency f_c are larger in the short resonator (2.3 GHz) making k larger, increasing the nonuniformity per unit length. In contrast, the longer resonator has a small deviation of f from f_c and a smaller k, but is more sensitive to changes along the length, kl, making the

nonuniformity more apparent (Eq. (13)). The total fractional rf magnetic field nonuniformity from center to end is given by $1-\cos^2 kl$. It is expected that as the length becomes greater than one FS wavelength, the resonator will become very phase sensitive, large kl, and will require trimming of the end sections.

The results of this paper are parallel to previous work from this laboratory [9–11]. They show that a LGR can be viewed as a strongly reentrant ridged waveguide at cutoff. With this analogy, the family of uniform field cavities is extended to include LGRs.

Acknowledgments

This work was supported by grants EB001417, EB001980 and EB002052 from the National Institutes of Health. We thank Wojciech Froncisz for suggesting to us that an LGR might be considered as a resonator at cutoff.

References

1. Froncisz W., Hyde J.S.: J. Magn. Reson. **47**, 515–521 (1982)
2. Hyde J.S., Froncisz W. in: Advanced EPR: Applications in Biology and Biochemistry (Hoff A.J., ed.), pp. 277–306. Amsterdam: Elsevier 1989.
3. Rinard G.A., Eaton G.R. in: Biomedical EPR. Part B: Methodology and Instrumentation. Biological Magnetic Resonance, vol. 24 (Eaton S.S., Eaton G.R., Berliner L.J., eds.), pp. 19–52. New York: Kluwer Academic/Plenum 2004.
4. Froncisz W., Oles T., Hyde J.S.: Rev. Sci. Instrum. **57**, 1095–1099 (1986)
5. Hyde J.S., Yin J.-J., Subczynski W.K., Camenisch T.G., Ratke J.J., Froncisz W.: J. Phys. Chem. B **108**, 9524–9529 (2004)
6. Robins W.P.: Phase Noise in Signal Sources, p. 53. London: Peter Peregrinus Ltd. 1982.
7. Hyde J.S., Sidabras J.W., Mett R.R. in: 46th Rocky Mountain Conference on Analytical Chemistry, Denver, CO, August 1–5, 2004, pp. 84–85.
8. Froncisz W., Hyde J.S.: J. Magn. Reson. **47**, 515–521 (1982)
9. Mett R.R., Froncisz W., Hyde J.S.: Rev. Sci. Instrum. **72**, 4188–4200 (2001)
10. Anderson J.R., Mett R.R., Hyde J.S.: Rev. Sci. Instrum. **73**, 3027–3037 (2002)
11. Hyde J.S., Mett R.R., Anderson J.R.: Rev. Sci. Instrum. **73**, 4003–4009 (2002)
12. Jackson J.D.: Classical Electrodynamics, 2nd edn. New York: Wiley 1975.
13. Smythe W.R.: Static and Dynamic Electricity, 2nd edn., chapt. IV. New York: McGraw-Hill 1950.
14. Ramo S., Whinnery J.R., van Duzer T.: Fields and Waves in Communication Electronics, 2nd edn., sect. 1.18. New York: Wiley 1984.
15. Hyde J.S., Yin J.-J., Subczynski W.K., Camenisch T.G., Ratke J.J., Froncisz W.: J. Phys. Chem. B **108**, 9524–9529 (2004)
16. Mett R.R., Sidabras J.W., Hyde J.S. in: 48th Rocky Mountain Conference on Analytical Chemistry, Breckenridge, CO, July 23–27, 2006.
17. Pennington P.M., Hyde J.S. in: 48th Rocky Mountain Conference on Analytical Chemistry, Breckenridge, CO, July 23–27, 2006.
18. Mett R.R., Hyde J.S.: J. Magn. Reson. **165**, 137–152 (2003)

Authors' address: James S. Hyde, Department of Biophysics, Medical College of Wisconsin, 8701 Watertown Plank Road, Milwaukee, WI 53226-0509, USA
E-mail: jshyde@mcw.edu